Computers & Fluids 38 (2009) 1925–1942

Contents lists available at ScienceDirect

Computers & Fluids

journal homepage: www.elsevier.com/locate/compfluid

Computation of circulation control airfoil flows

R.C. Swanson *, C.L. Rumsey

NASA Langley Research Center, Computational AeroSciences Branch, 15 Langley Blvd., Hampton, VA 23681-2199, USA

ARTICLE INFO

Article history:
Received 21 October 2008
Received in revised form 18 March 2009
Accepted 22 May 2009
Available online 28 May 2009

ABSTRACT

The compressible Reynolds-averaged Navier–Stokes equations are solved for circulation control (CC) airfoil flows. Three turbulence models are considered for closure, including the Spalart–Allmaras model with and without a curvature correction and the shear stress transport model of Menter. Numerical solutions are computed with a structured grid solver. The effect of mesh density on the solutions is examined. We also address two important issues that have emerged in simulations of CC airfoil flows. One is the validity of incompressible simulations with the presence of a transonic wall jet. The other issue concerns the occurrence of nonphysical solutions for CC airfoil flows. In the present work we consider circulation control flows for a range of jet momentum coefficients. Comparisons are made between computed and experimental pressure distributions, velocity profiles, Reynolds stress profiles, and streamline patterns. Including curvature effects yields the closest agreement with the measured data.

Published by Elsevier Ltd.

1. Introduction

Flow control offers a multitude of opportunities to improve not only aerodynamic performance but also safety and environmental impact of flight vehicles [1]. Circulation control (CC) is one type of flow control that is currently receiving considerable attention. Such flow control is usually implemented by tangentially injecting a jet sheet over a rounded wing trailing edge. The jet sheet remains attached farther along the curved surface of the wing due to the Coanda effect (i.e., a balance of the pressure and centrifugal forces). This results in the effective camber of the wing being increased, which produces lift augmentation. A CC configuration offers the possibility of reduced take-off and landing speeds as well as increased maneuverability. Further, the use of pulsed jets with CC systems, as discussed by Jones and Englar [2], provides the possibility of significantly reducing the mass flow required to achieve a desired performance, a principal obstacle to the installation of CC systems on production aircraft.

Computational methods will play a vital role in designing effective CC configurations. Due to the cost of flow control experiments, design and parametric studies will strongly depend on accurate and efficient prediction methods. An effective computational technique for CC flows must be able to appropriately represent the characteristics of the jet flow (e.g., jet spreading rate) and the exchange of momentum between the jet and the outer flow. This is an especially challenging requirement, since there are multiple length scales that characterize the physics of the turbulent flow over a circular trailing edge (Coanda surface). These length scales are associated with the boundary layer upstream of the jet slot, the Coanda surface boundary layer, the wall jet, and the shear layer between the jet and external flow. To capture the multiscale turbulent flow phenomena, and at the same time restrict the required computational effort so as to not preclude the possibility of using the computational method for design, the Reynolds-averaged Navier–Stokes (RANS) equations are currently being solved for CC flow problems. The RANS equations require a turbulence model for closure. Thus, a major difficulty in constructing an effective method for computing CC flows is finding a turbulence model that can adquately represent the various salient scales.

At the circulation control workshop [3] held at NASA Langley in 2004, an effort was made to assess the current capability to calculate CC airfoil flows. Although the assessment included a wide range of applications, the focus was the computation of the flow over the CC airfoil configuration (NCCR 1510-7067) tested by Abramson [4]. Various computational methods and a variety of turbulence models, ranging from an algebraic model to a full Reynolds stress model, were considered. Predicted pressure distributions were compared with experimental pressure data. The range of numerical solutions presented underscored the importance of computational grid and turbulence modeling in predicting such complex turbulent flows. In addition, different results were frequently obtained with nominally the same turbulence model. The need to clearly identify the version of a given turbulence model being used was evident, especially since relatively simple changes in a model can have a dramatic impact on the flow solution. Furthermore, specific delineation of the implementation details (e.g., type of discretization and numerical approximation of various terms) of the model should also be given, since this can affect the behavior of the model.

* Corresponding author. Present address: Center of Computer Applications in AeroSpace Science and Engineering, ($C^2A^2S^2E$) in Braunschweig, Germany. Tel.: +1 757 864 2165; fax: +1 757 864 8816.
E-mail address: r.c.swanson10@gmail.com (R.C. Swanson).

0045-7930/$ - see front matter Published by Elsevier Ltd.
doi:10.1016/j.compfluid.2009.05.002

Nomenclature

a	speed of sound
b	wing span
C_D	section drag coefficient, $D/(q_\infty A)$
C_f	surface skin friction coefficient, τ_w/q_∞
C_L	section lift coefficient, $L/(q_\infty A)$
C_p	pressure coefficient, $(p-p_\infty)/q_\infty$
C_μ	jet momentum coefficient, $(\dot{m}U_j)/(q_\infty A)$
c	chord length
c_{r3}	parameter for curvature effects
d	distance normal to airfoil surface
h_L	lip height of jet slot
h_P	plenum inlet height
h_S	jet slot height
k	turbulent kinetic energy
M	Mach number, U/a
$\dot{m}$	mass flow rate
p	pressure
q	dynamic pressure, $(\rho U^2)/2$
r_{te}	radius of circular trailing edge
R	gas constant
Re	Reynolds number, $(\rho U_\infty c)/\mu$
S	wing planform area
T	temperature
U	velocity
u_{parallel}	mean tangential velocity component
u_τ	friction velocity, $\sqrt{\tau_w/\rho}$
u', v'	fluctuating velocity components (tangential and normal)
$-\overline{u'v'}$	specific Reynolds stress
x, y	cartesian coordinates
y^+	normalized coordinate, $(y u_\tau)/\nu$

Greek

α	angle of attack
γ	specific heat ratio
ϵ	dissipation rate of k
ζ	enstrophy
θ	angle relative to start of airfoil trailing edge (upper surface)
μ	coefficient of viscosity
ν	kinematic viscosity
ρ	density
τ	shear stress
ω	specific dissipation rate of k, k/ν_t

Subscript

c	based on chord length
exp	refers to experiment
j	jet condition
ref	reference (∞) condition
t	turbulent flow quantity
w	solid surface (wall) condition
0	total condition
∞	free-stream quantity

In a paper [5] presented at the workshop we applied the compressible Navier–Stokes solver CFL3D [6] in computing the flow over the CC airfoil geometry in the experiment of Abramson and Rogers [7]. This airfoil geometry very closely approximates that of the Abramson [4] experiment, as revealed in a direct comparison of the two geometries shown in Swanson et al. [5]. Calculations were performed for the two low Mach number ($M = 0.12$) cases of the workshop, having angles of attack (α's) equal to 0° and −8°, as well as for a $M = 0.6$ case. With the Spalart–Allmaras (SA) turbulence model [8] that includes curvature effects, which is designated the SARC model [9], reasonably good agreement was obtained with the measured pressure data for the two Mach number cases. However, an unusually large value of the curvature correction parameter seemed to be necessary for the SARC model. Calculations were also performed with other turbulence models. For the low Mach number cases the surface pressures computed with the shear stress transport (SST) model of Menter [10] compared fairly well with the experimental data. The SST model exhibited sensitivity to changes in the modeling of the turbulence production term (i.e., use of vorticity or strain rate). In fact when using vorticity in the production term, the jet failed to separate on the Coanda surface for the $\alpha = 0°$ case, and it moved onto the lower (pressure) surface of the airfoil before separating. Whenever, the jet travels around the entire Coanda surface and begins to traverse the lower surface of the airfoil, we designate this behavior as "jet wrap-around." For the $M = 0.6$ case, the surface pressures calculated with the SA, SST, and the explicit algebraic Reynolds stress (EASM) model in 1988 Wilcox $k-\omega$ form (EASM-ko) [11] compared poorly with the data. There was a clear need for further investigation of these turbulence models as well as others.

For the workshop cases Fasel et al. [12] has also obtained fairly good agreement with the surface pressure data when solving the RANS equations and using the EASM model in conjunction with either the 1988 or 1998 versions of the $k-\omega$ models [13,14]. They did not indicate steady-state convergence criteria, which can be an issue with this model. We should point out that in our experience converged solutions (i.e., residuals reduced at least five orders of magnitude) are generally difficult to attain with the EASM (with $k-\omega$) model. Fasel et al. also performed calculations with the 1988 $k-\omega$ and Menter SST models. They observed jet wrap-around with both models. Details of their implementation of these models were not given. As indicated previously, Swanson et al. [5] demonstrated that results with and without jet wrap-around can be obtained when using the Menter SST model, depending upon whether vorticity or strain rate is used in the computation of the turbulence production term. This is a good example of why it is important to provide at least the salient details of the implementation of the model.

Chang et al. [15] solved the steady RANS equations for the CC airfoil of the 2004 workshop. They considered both circular and logarithmic spiral trailing edges as well different slot heights, blowing rates, and angles of attack. Solutions were obtained with the compressible segregated solver of the finite-volume code Fluent. This solver uses the SIMPLE pressure–velocity coupling. To model turbulence Chang et al. applied the SST model of Menter and the full Reynolds stress (FRS) model of Launder et al. [16]. For the circular trailing edge CC airfoil the trends of the computed results compared well with the experimental data, but generally the circulation was lower than that of the experiment, which reflected the underprediction of the aft end suction peak and the upper surface suction levels. Under all flow conditions physically realistic solutions were obtained. However, this was not the case with the logarithmic spiral trailing edge, which has a constantly increasing radius of curvature with the smallest radius at the jet slot. Even with the FRS model jet wrap-around occurred when the jet momentum coefficient $C_\mu \geqslant 0.08$.

With the purpose of providing data for Navier–Stokes validation, Novak et al. [17] used two-dimensional laser doppler velocimetry to obtain detailed flow-field data for the low speed flow over a 15.6% thick CC airfoil geometry with a supercritical leading edge and circular trailing edge. Extensive flow-field surveys, including velocity and Reynolds stress profiles, were taken on the aft section of the airfoil for two values of the jet momentum coefficient. To date this data set is the most comprehensive available for CC flows. Previously, Shrewsbury [18,19] and Viegas et al. [20] solved the compressible RANS equations and made comparisons primarily with experimental pressure data and streamlines. By varying the angle of attack for the computations until the experimental lift coefficient was matched, Shrewsbury obtained computed pressures that compared well with the measured pressure data. In these calculations the mixing length of the algebraic eddy viscosity model of Baldwin and Lomax [21] was modified by an empirical curvature correction.

Viegas et al. attempted to eliminate some of the uncertainties associated with wind tunnel wall corrections by including lower and upper tunnel walls in a two-dimensional simulation of the Novak et al. experiment. With this approach they could only account primarily for blockage effects, since the wing model in the experiment was mounted between the two sidewalls of the tunnel. An angle of attack correction was not used. Several versions of the Baldwin–Lomax and the two-equation Jones–Launder models, with and without curvature corrections, were considered. Since the important interference effects produced by the tunnel sidewalls (e.g., reduction in effective angle of attack) were not taken into account, there were significant differences between computed and experimental pressure distributions on the suction surface of the airfoil.

More recently (2005) Swanson et al. [22] computed solutions for the CC airfoil flows of the Novak et al. experiment. They solved the RANS equations and applied several turbulence models to determine their effects on the flow field. Results with the SA, SARC (SA model with rotation and curvature corrections), and SST models as well as the k-enstrophy $(k-\zeta)$ model of Robinson and Hassan [23] were compared with the experimental data. The closest agreement with the data was obtained with the SARC model. Even with fairly good agreement with surface pressures, jet separation location on the Coanda surface, and generally for the velocity profiles, there was still an overprediction of the lift coefficient for low and medium blowing coefficients ($C_\mu = 0.03, C_\mu = 0.10$) of about 12%. The greatest differences between the predicted and experimental C_L occurred at the highest C_μ considered ($C_\mu = 0.226$), with the computed value being nearly 30% higher. Only the SARC model allowed physically correct solutions for the full range of C_μ considered. For example, at and above $C_\mu = 0.10$ there was jet wrap-around in results with the SST model.

In 2006 some simulations were performed for the CC airfoil of the Novak experiment using two incompressible flow codes. Baker and Paterson [24] used the CFDSHIP code [25] and the AcuSolve code [26] to solve the incompressible RANS equations. The CFDSHIP code is based on a finite-difference formulation for overset grids, and the AcuSolve code is based on a finite-element approach (see Shakib [27]). To represent the effects of turbulence they used the SST model with the CFDSHIP code and the SA model modified for curvature effects with the AcuSolve code. In all simulations they used the geometric α rather than the effective α. We should point out that for the Novak experiment there were signficant α corrections due to wind tunnel effects. Thus, free-air computations require the effective α. Baker and Paterson compared computed surface pressures and velocity profiles with the experimental data for $C_\mu = 0.03$ and $C_\mu = 0.10$. Over the forward sections of the airfoil their results actually showed a fairly good agreement with measured surface pressures. However, in all calculations they obtained significantly lower suction peaks than the experiment on the aft section of the airfoil. This underprediction of the suction peak is not surprising in light of the fact that the incompressible RANS equations were solved. For the two values of C_μ the computed jet exit velocity either essentially matches or slightly exceeds (rather than underpredicting) the experimental one; and thus, the incompressibility of the equations would explain why the acceleration of the flow is not being correctly predicted. The reduced trailing edge acceleration is accompanied by a reduced circulation, which compensates for the effect of using the geometric α and allows fairly good agreement with measured pressure data on the forward sections of the airfoil.

Even with incompressibility effects on the solutions and the use of the uncorrected α, Baker and Paterson actually obtained for $C_\mu = 0.03$ reasonably good agreement between some of the calculated (with AcuSolve code) and measured mean tangential velocity profiles on the Coanda surface. The velocity comparisons were not nearly as good for $C_\mu = 0.10$, especially since the computed jet flow separation occurred much sooner than that of the experiment. Based on these CC airfoil results and others with similar geometry and flow conditions Baker and Paterson concluded that RANS methods have sufficient accuracy and reliability that they can be used as a design tool for CC airfoils. As we will demonstrate in this paper, such a conclusion based upon incompressible simulations with the presence of transonic jets is not appropriate. Furthermore, such a conclusion does not reflect the current capability for accurate and efficient computation of CC solutions for a wide range of flow conditions and geometries.

Pfingsten et al. [28] computed the $C_\mu = 0.03$ and $C_\mu = 0.10$ cases of the Novak experiment to validate their CC airfoil prediction capability. They used the hybrid unstructured, compressible RANS flow solver of the TAU code [29]. For all calculations they used a mesh of about 1×10^5 points with quadrilaterals in the viscous region and triangles elsewhere. Solutions were computed with the effective α. The SA model and two variations to account for curvature effects were considered for modeling turbulence. Pfingsten et al. compared computed surface pressure distributions and velocity profiles on the Coanda surface with the Novak data. They obtained good predictions of the jet separation location for both C_μ values. Also, the velocity profiles presented, which were calculated with the SARC model, compared well with the data and the results of Swanson et al. [22].

In the current work we make detailed comparisons of numerical solutions with the extensive flow-field measurements of the Novak et al. experiment. The purpose of the work is not only to assess the numerical prediction capability of a representative RANS solver for CC airfoil flows but also to further investigate the effects of turbulence modeling on the flow field. The SA, SARC, and SST transport-type equation models are considered. We examine the effect of grid density on the solutions. In addition, several issues that have emerged in simulations of CC airfoil flows are addressed. For example, the validity of an incompressible simulation with the presence of a transonic wall jet is examined. We demonstrate that a reasonably good prediction of the surface pressure distribution can be obtained (except for the trailing edge suction peak) when solving the incorrect problem. Another issue is the occurrence of a physically unrealistic result such as jet wrap-around at higher blowing coefficients. The nature of such behavior is examined. Sometimes jet wrap-around results can be prevented by increasing the tangential resolution on the Coanda surface, and this will be discussed. In the present work comparisons are also made between computed and experimental pressures, velocity and Reynolds stress profiles, and streamline patterns. The effect of streamline curvature is demonstrated by comparing results computed with the SA and SARC models.

The initial sections of the paper concern the CC airfoil geometry and flow conditions, description of grids, numerical method, and boundary conditions. This is followed by a section on turbulence modeling, where emphasis is given to the implementation details of the models that can significantly affect their performance. In the final two sections the numerical results are presented and discussed, and concluding remarks are given.

2. Geometry and flow conditions

The circulation control wing (CCW) model in the Novak et al. experiment has a chord of 38.18 cm and a span of 60.96 cm, resulting in an aspect ratio of 1.6. The CC airfoil section (see Fig. 1) has a supercritical leading edge, symmetric middle section, and a 5.08 cm diameter Coanda CC aft section. It has a thickness ratio of 15.6%. The jet slot height to chord ratio is 0.002, which corresponds to $h_S = 0.762$ mm, and the $h_S/r_{te} = 0.03$. The height of the jet slot lip is 0.61 mm. At the inlet of the plenum the height is 2.06 cm.

For the tests conducted by Novak et al. the free-stream Mach number is 0.12, and the Reynolds number based on chord is 0.986×10^6. The geometric angle of attack is 0°. The values of the jet momentum coefficient, which is the ratio of the jet momentum to the free-stream momentum, for which two-dimensional laser velocimeter (LV) data were taken on the Coanda surface are 0.03 and 0.10. The ratios of the jet exit velocity to the free-stream velocity corresponding to $C_\mu = 0.03$ and $C_\mu = 0.10$ are 3.44 and 5.69, respectively.

Of particular concern in performing numerical computations is having the boundary conditions that are actually present in the experiment. The parameter C_μ is an important quantity in circulation control experiments since it is used to determine the plenum inflow boundary conditions needed to give the correct jet exit conditions. Usually, the C_μ is calculated in one of the following two ways:

$$C_\mu = \frac{\dot{m}_j U_j}{q_\infty S}, \qquad C_\mu = \frac{\rho_j U_j^2 h_S b}{\frac{1}{2}\rho_\infty U_\infty^2 c b},$$

where $\dot{m}_j$ is the measured mass flux. The jet velocity U_j is determined by isentropically expanding the plenum flow to the free-stream static pressure. Thus, U_j can be calculated from

$$U_j = \left[2\frac{\gamma R T_0}{\gamma - 1}\left(1 - \left(\frac{p_\infty}{p_0}\right)^{\frac{\gamma-1}{\gamma}}\right)\right]^{\frac{1}{2}}. \tag{2.1}$$

In the Novak experiment the first method is used for calculating C_μ because it is more accurate, as it does not depend directly on the slot height h_S. The U_j computed in this manner is expected to be somewhat lower than the actual value since the jet exit pressure is usually less than the free-stream pressure. It should be pointed out that the airfoil trailing edge radius to chord ratio of 0.067 is large and not representative of practical flight systems. This value was used to enable larger physical slot heights, allowing improved spatial resolution for the LV measurements in the trailing edge region. Moreover, with this choice the jet exit velocity could be measured with a higher degree of accuracy. Having this measurement is quite important for verifying that the plenum inflow conditions are indeed producing the required U_j and establishing the jet flow in the computations correctly.

Although the experiment was designed to be two-dimensional, there are three-dimensional effects due to the presence of the sidewalls in the wind tunnel. Interference effects are imposed on the flow field by separation and roll-up of the sidewall boundary layers. The separation of the boundary layers in the wing/sidewall juncture regions is a consequence of one or more strong adverse pressure gradients on the upper surface of the wing. These circumstances are further complicated by the high circulation around the CC wing that must decrease as the sidewalls are approached, generating vortex shedding (like that of a finite wing). These vortical structures induce a downwash along the span of the wing, reducing the effective angle of attack. For the C_μ values being considered in this paper the angle of attack corrections suggested by the experimenters are given in Table 1. These corrections were estimated (see Novak and Cornelius [30]) with the procedure of Wood and Rogers [31], which is based on the assumption that the pitching moment as a function of lift is a constant in free air. Since the α corrections, due to downwash caused by sidewall vortical structures, are relatively large and difficult to determine experimentally with high confidence, an effort was made in this study to assess the influence of the correction on the pressure distribution. Unless otherwise noted, all two-dimensional computational

Table 1
Angle of attack correction.

C_μ	α_{cor}(deg)
0.030	−2.46
0.100	−5.86
0.226	−8.94

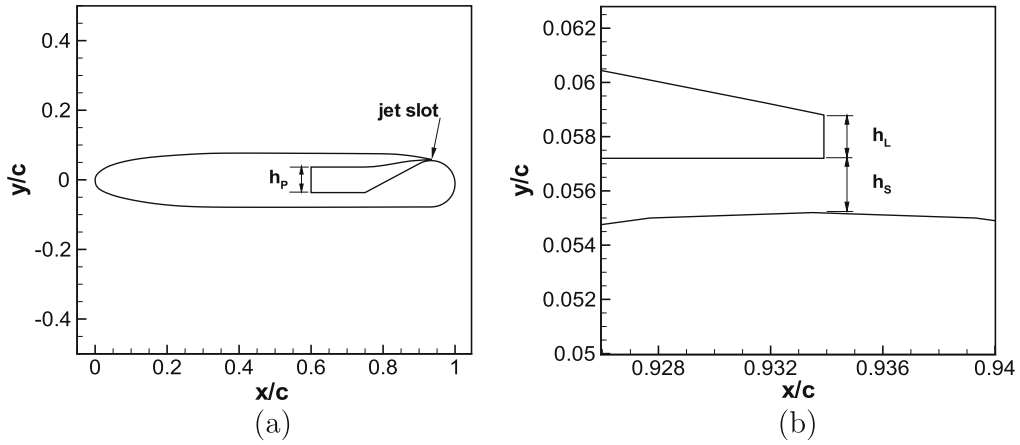

Fig. 1. Geometry of Novak et al. experiment based on measured coordinates. (a) CC airfoil and (b) jet slot and lip.

results presented in this paper applied the corrected angle of attack.

Estimates of the errors in the LV data were made by Novak et al. for the experiment. The error for the mean velocities was estimated to not exceed 2%. For the turbulence intensities the error is between 3% and 5%, and for the shear stresses it is between 10% and 25%.

3. Computational grids

For the numerical computations multi-block structured grids with O-type topology were used. To assess the effects of mesh resolution a set of grids was generated. Starting with a fine grid, containing 303,936 points, a medium mesh was obtained by eliminating every other mesh line. In the same manner a coarse grid was generated starting on the medium mesh. The coarse, medium and fine grids are designated as grid 5c, grid 5m, and grid 5f, respectively. The "5" delineates an internal designation of a particular grid series.

The discretized domain was partitioned into six blocks, as shown in Fig. 2, which displays the near field of the coarse resolution grid. The thick lines in the figure indicate block interface boundaries. At the interface boundary in the region below the airfoil the grid was patched, as seen in Fig. 2. The fine grid contains 1185 points around the airfoil and 161 points in the the normal direction over the forward part of the airfoil. Over the aft part of the airfoil there are 289 points in the normal direction, with 81 points over the length of the plenum for the jet. The grid is tangentially clustered at the airfoil leading and trailing edges. A typical streamwise spacing on the Coanda surface is 4×10^{-4}. The grid is also clustered in the normal direction near the walls in order to resolve the turbulent boundary layers. In the normal direction the grid spacing at the wall is 1×10^{-5} giving an average normalized coordinate y^+ that is less than one for the first grid point off the wall boundary. The quantity y^+ is the standard law of the wall coordinate. To adequately represent the effect of the vortex behind the lip of the jet slot the normal spacing near the lip surface is 1×10^{-5}, and the lip is treated as a viscous surface. The outer boundary is located 40 chords away from the airfoil boundary.

4. Numerical methods

Numerical solutions on the structured grid were computed with CFL3D, a multi-zone Reynolds-averaged Navier–Stokes (RANS) code developed at NASA Langley [6]. It solves the thin-layer form of the compressible RANS equations in each of the (selected) coordinate directions. It can use one-to-one, patched, or overset grids, and employs local time step scaling, grid sequencing, and multigrid to accelerate convergence to steady state. In time-accurate mode, CFL3D has the option to employ dual-time stepping with subiterations and multigrid, and it achieves second-order temporal accuracy.

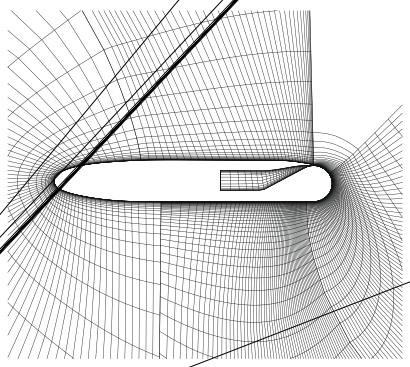

The code CFL3D is based on a finite-volume method. The convective term is approximated with third-order upwind-biased spatial differencing, and the pressure and viscous terms are discretized with second-order central differencing. The discrete scheme is globally second-order spatially accurate. The flux difference-splitting (FDS) method [32] of Roe is employed to obtain fluxes at the cell faces. Advancement in time is accomplished with an implicit approximate factorization method (number of factors determined by number of dimensions).

In CFL3D, the mean-flow and turbulence modeling equations are solved in a loosely coupled manner. This means that the iterative procedure for the mean-flow equations is advanced one pseudo-time step, and then the iterative process for the equation(s) of the turbulence model is advanced one pseudo-time step. Each turbulent transport equation is solved using an implicit approximate factorization approach. The advection terms are discretized with first-order upwind differencing. The production source term is treated explicitly, while the advection, destruction, and diffusion terms are treated implicitly.

For all calculations the discrete L_2 norm of the residual of the continuity equation was reduced between 6 and 7 orders of magnitude. This ensured that the computed aerodynamic coefficients were converged to at least three significant digits. With the SA and SARC turbulence models solutions were obtained with full multigrid (FMG). Moreover, solutions were calculated with multigrid on three successive grids, each one being a proper subset of the next finer grid. With the SST model the convergence with multigrid sometimes stalled, and the residual was not reduced to an acceptable level. Under this circumstance we simply discontinued the multigrid and proceeded with a single grid calculation until the residual was reduced more than six orders. When jet wrap-around occurred the residual reduction criterion could not be satisfied.

5. Boundary and initial conditions

Boundary conditions are required at the inflow (internal and external), outflow, and solid surface boundaries. For numerical computations the physical boundary conditions must be supplemented with numerical boundary conditions, which generally involve extrapolation of flow quantities or combinations of them (e.g., Riemann invariants) from the interior of the domain. Discussion of the numerical boundary conditions is given in the user's manual for CFL3D [6]. At the far-field inflow boundary a Riemann invariant, entropy, and flow inclination angle are specified. A Riemann invariant is specified at the far-field outflow boundary. At the upstream wall of the plenum the following conditions are prescribed in the current study: for $C_\mu = 0.03$, $u/a_\infty = 0.00950$; for $C_\mu = 0.10$, $u/a_\infty = 0.01370$; for $C_\mu = 0.226$, $u/a_\infty = 0.01514$. Here a_∞ is the free-stream speed of sound. At the surface boundaries the no-slip and adiabatic wall conditions are specified. Boundary conditions for the various turbulence models considered herein are given in [6]. The initial solution is either defined by the free-stream conditions or a coarser grid solution.

6. Turbulence modeling

In all the CC airfoil flows the computations are performed fully turbulent; several turbulence models are considered. Two of the models are the SA model and the SARC model [9,33], which is the SA model with rotation and curvature corrections. The other model for the effects of turbulence is the SST model of Menter

[10,34,35]. All of these models are linear eddy-viscosity models that make use of the Boussinesq eddy-viscosity hypothesis. The equations describing these three models can be found in their respective references. However, there are certain details concerning the implementation of the SARC and SST models that are given here in order to precisely identify what form of the model is being applied.

The SA model can be written in general form as

$$\frac{D\tilde{\nu}}{Dt} = \mathcal{P} + \mathcal{D}_{diff} + \mathcal{D}_{diss} \tag{6.1}$$

where $\tilde{\nu} \sim \nu_t$, and $\mathcal{P}$, $\mathcal{D}_{diff}$, and $\mathcal{D}_{diss}$ are the contributions associated with turbulence due to production, diffusion, and dissipation, respectively. The production term is given by

$$\mathcal{P} = c_{b1}[1 - f_{t2}]\Omega\tilde{\nu}, \tag{6.2}$$

with Ω being the magnitude of the vorticity. In the SARC model $\mathcal{P}$ is replaced by

$$\mathcal{P}' = c_{b1}[f_{r1} - f_{t2}]\Omega\tilde{\nu}, \tag{6.3}$$

$$f_{r1} = (1 + c_{r1})\frac{2r^*}{(1 + r^*)}\left[1 - c_{r3}\tan^{-1}(c_{r2}\tilde{r})\right] - c_{r1}, \tag{6.4}$$

where the function r^* is the ratio of scalar measure of strain rate to the scalar measure of rotation, the function $\tilde{r}$ depends on the Lagrangian derivative of the strain-rate tensor principal axes angle (see [33] for details), and $c_{r1} = 1$, $c_{r2} = 12$, and $c_{r3} = 0.6 - 1.0$. As c_{r3} is increased, the turbulence production will decrease near convex surfaces. In the results for this paper we use $c_{r3} = 1.0$.

The production term $\mathcal{P}_k$ in the turbulent kinetic energy equation of the Menter SST model can be written as

$$\mathcal{P}_k = \tau_{ij}\frac{\partial u_i}{\partial x_j}, \tag{6.5}$$

where the stress tensor τ_{ij} is defined as

$$\tau_{ij} = \mu_t\left(\frac{\partial u_i}{\partial x_j} + \frac{\partial u_j}{\partial x_i} - \frac{2}{3}\frac{\partial u_k}{\partial x_k}\delta_{ij}\right) - \frac{2}{3}\rho k\delta_{ij}, \tag{6.6}$$

and the partial derivatives are strain rates. The production term $\mathcal{P}_\omega$ in the ω equation of the SST model is proportional to $\mathcal{P}_k$. Generally, in the computations with the SST model, the incompressible assumption is imposed, and the turbulent kinetic energy contribution in Eq. 6.6 is neglected. Thus,

$$\mathcal{P}_k \approx \mu_t\left(\frac{\partial u_i}{\partial x_j} + \frac{\partial u_j}{\partial x_i}\right)\frac{\partial u_i}{\partial x_j} = 2\mu_t S_{ij}S_{ij}, \tag{6.7}$$

where the strain-rate tensor S_{ij} is given by

$$S_{ij} = \frac{1}{2}\left(\frac{\partial u_i}{\partial x_j} + \frac{\partial u_j}{\partial x_i}\right), \tag{6.8}$$

and $S_{ij}S_{ij}$ means the scalar (or double dot) product of two tensors. Note that it is also common as a further approximation to employ the vorticity rather than the strain-rate tensor (see Menter [34]). In the present work we use Eq. 6.7 for $\mathcal{P}_k$.

The eddy viscosity determined with the SST model is defined as

$$\nu_t = \frac{a_1 k}{max(a_1\omega; \Omega F_2)}, \tag{6.9}$$

where a_1 is a constant, ω is equal to the ratio of the turbulent dissipation rate to the turbulent kinetic energy, $\Omega = \sqrt{2W_{ij}W_{ij}}$ with W_{ij} denoting the rotation tensor, and F_2 is a blending function.

7. Numerical results

The computational methods described in previous sections were applied to three CC airfoil flow cases from the Novak et al. experiment. As indicated previously the Mach number for all cases is 0.12, and the Reynolds number is 0.986×10^6. The jet momentum coefficients for these cases are 0.03, 0.10, and 0.226, and the corresponding effective angles of attack are given in Table 1. For the first two cases there are detailed measured data on the Coanda surface, and comparisons with the velocity and shear stress profiles are made. In all cases the computed and experimental pressures are compared.

7.1. Low jet momentum coefficient ($C_\mu = 0.03$)

In the first part of this section we examine several different effects on the solution for the flow over a CC airfoil. The effects include the following: grid density on the magnitude of the suction peak on the Coanda surface, angle of attack correction, and reduction of C_μ when α is not corrected. By considering the latter effect we indicate how apparent good comparisons with experimental surface pressures can be obtained even when solving the wrong problem. This result has direct implications regarding the simulation of CC airfoil flows with transonic jets using the incompressible RANS equations.

A series of computations with $C_\mu = 0.03$ were performed on the set of three grids generated with grid 5. As indicated previously the mesh spacing of the coarse grid (grid 5c) is a factor of four smaller in each coordinate direction than that of the fine grid (grid 5f). In Fig. 3(a) we see that there are relatively small differences between the computed pressure distributions on the three grids. Furthermore, there is essentially no difference in the suction peak on the aft section (Coanda surface) of the airfoil. The computed surface pressure distribution exhibits fairly good agreement with the experimental data, although the suction peak prediction on the airfoil aft section is somewhat high.

Fig. 3(b) compares the surface pressures calculated with the nominal α of 0° and the corrected (or effective) α of −2.46°. This figure shows the expected higher suction peak at the leading edge of the airfoil when using the uncorrected α. In addition, we see that there is essentially no change in the suction peak on the Coanda surface. Such behavior is characteristic of airfoil calculations with modest variations in α.

In Fig. 3(c) the effect of varying the C_μ on the pressure distribution is displayed. For these calculations the nominal α was used, and the C_μ was decreased by 40% (which corresponds to a magnitude change in the plenum inflow velocity of 20%) relative to $C_\mu = 0.03$. The figure shows that as the C_μ is decreased we obtain an overall increase in the upper surface pressures (decrease in pressure coefficient C_p) and decrease in the lower surface pressures (increase in C_p), along with accompaning lowering of the trailing edge suction peak. With the decrease in C_μ, the separation location of the jet from the Coanda surface occurs sooner. Fig. 3(d) displays the streamlines of the flow around the Coanda surface. There are two distinct vortices of comparable size formed behind the Coanda surface. As we will show later there are also two vortices present in the experiment; however, the upper vortex is much smaller than the lower one, which reflects the later jet separation than in the present result.

There are two primary comments concerning the effect of varying C_μ. First, a reasonably good prediction can be obtained over most of the airfoil for the surface pressures; and yet, the wrong problem is being solved because of the incorrect flow acceleration on the Coanda surface (i.e., emulating the effect of an incompressible simulation) and the neglect of the α correction. Second, since the flow acceleration on the Coanda surface is lower than it should be (i.e., when $C_\mu = 0.03$), then we are emulating what occurs for incompressible flow simulations. The reduced acceleration causes lower circulation, which explains partially the incompressible results of Baker and Paterson [24]. Moreover, using the Prandtl–

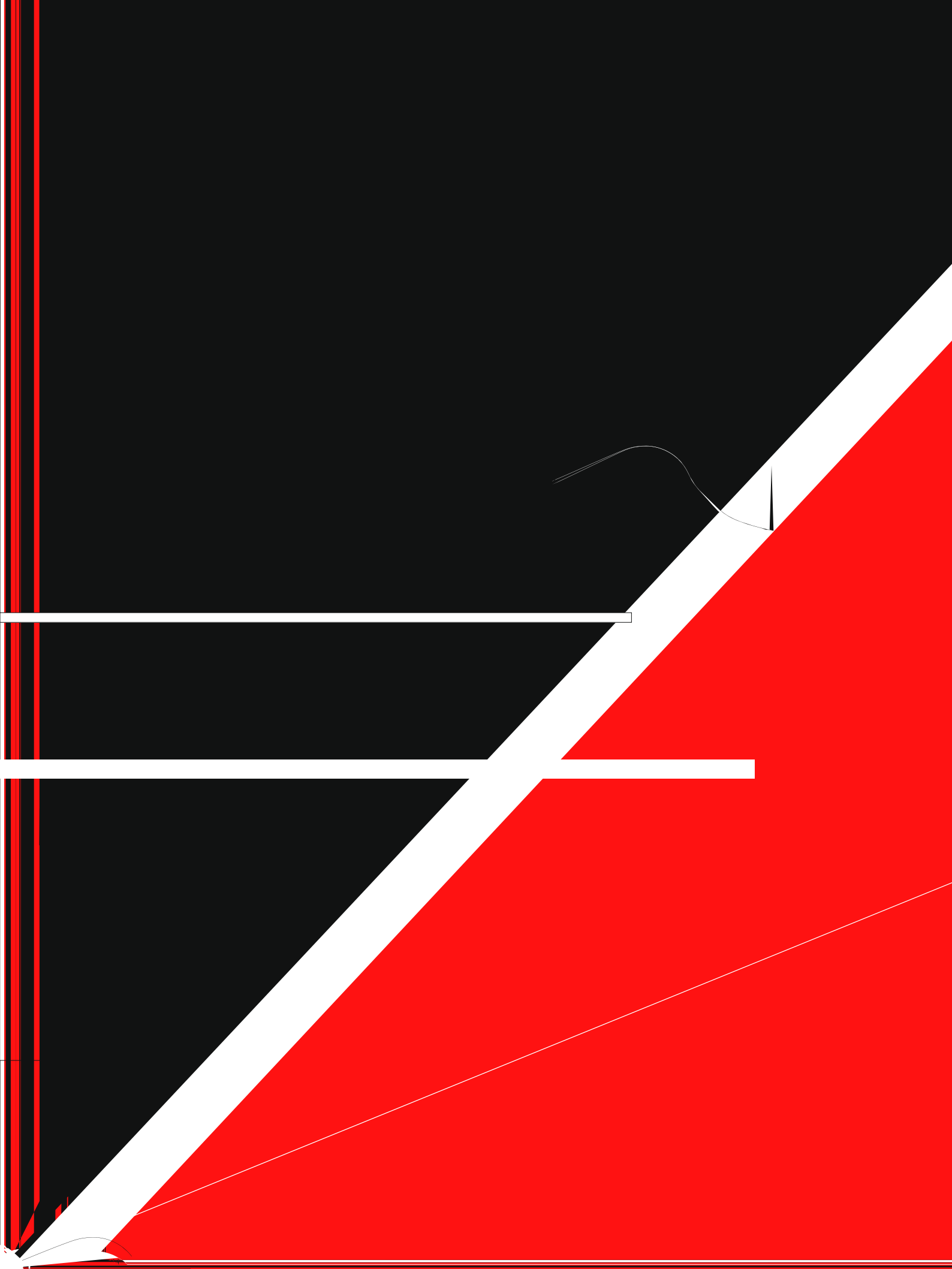

calculated on grid 5f with the SA, SARC, and SST models are displayed. The effect of grid refinement on the profiles obtained with the SARC model is also shown. Note that the local coordinate system, which is based on the tangential and normal directions, is applied in a clockwise manner, and that is why the u_{parallel} is negative on the lower surface. This is consistent with how the experimental data is given. On the upper and lower surfaces, the predicted velocity profiles with the three models are fairly close to each other, but they underpredict the data. The computed values are in the range of just 3–5% lower than the measured values on the upper surface, but they are roughly between 10% and 20% lower in absolute magnitude at the knee of the boundary-layer profile on the lower surface, where the magnitude of the velocities is half that on the upper surface. Such an underprediction, especially on the suction surface, is not expected, since this implies that the computational airfoil circulation is low, which would not be consistent with the somewhat low computed pressure level at $x/c = 0.875$. A possible explanation for this underprediction is that there were some spanwise variations in the jet conditions. As seen in Figs. 7(b) and 8(b) the calculated specific Reynolds stress profiles exhibit fairly good agreement with the data, with the greatest differences occurring in the vicinity of the peak value near the surface. On the upper surface the peak $-\overline{u'v'}$ occurs somewhat closer to the wall in the computations than it does in the experiment.

We now consider the flow over the Coanda surface. In Figs. 9(a–f) and 10(a–f), the velocity and shear stress profiles computed with the three models are compared with the corresponding measured data at six circumferential locations. Clearly, the SARC model provides the best agreement with the data. Generally, for the velocity profiles the agreement with the data is quite good. There is some disagreement with the measurements in the region of interaction between the jet flow and the outer shear layer at the $\theta = 50^\circ$ and $\theta = 80^\circ$ locations. At the $\theta = 90^\circ$ location there is a significant discrepancy between the predictions and data due to differences in the separated flow behavior. For the Reynolds stress profiles there is only fair agreement with the measured data, with the largest differences occurring in the vicinity of jet detachment.

7.2. Medium jet momentum coefficient ($C_\mu = 0.10$)

In Fig. 11(a) computed surface pressure variations for $C_\mu = 0.10$, corresponding to the three turbulence models, are compared with experimental data. The corrected α of -5.86° was used. The relative agreement with the data and the trends discussed for the $C_\mu = 0.03$ case are similar here. Moreover, the pressures computed with the SARC model are the closest to the experiment, again confirming the importance of representing the curvature effects. The pressure distributions with the SA and SST models nearly coincide, and they overpredict the suction levels on the upper surface. Fig. 11(b) shows the influence of mesh density on the surface pressures obtained using the SARC model. We see that there is little difference between the medium and fine grid results. In Fig. 12 the streamlines from the fine grid calculation with the SARC model

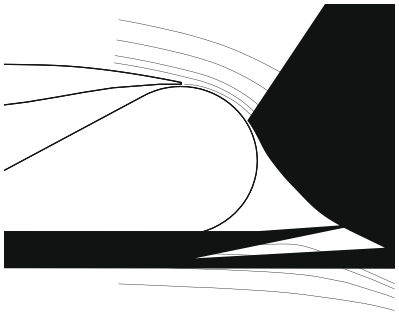

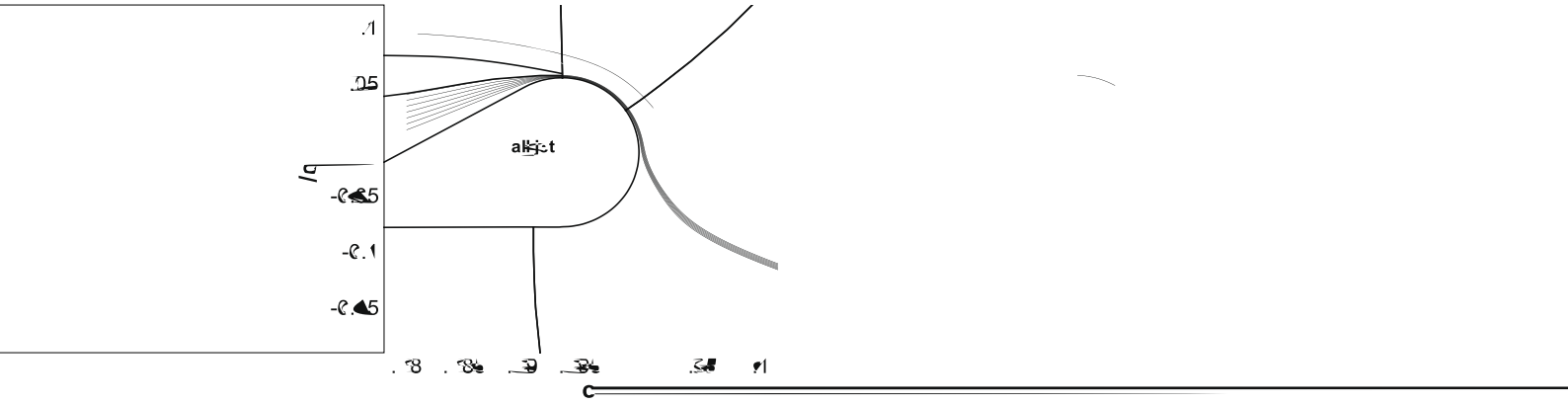

a)

are compared with those for the experiment. In the experiment the flow separates at the angular location $\theta \approx 115^\circ$. For the computed flow separation occurs at θ of about 112°. There is good agreement with the experimental streamlines. Although not perceptible in the figure, there is an extremely thin separation region on the lower surface of the airfoil near the trailing edge. Such a recirculation zone would not have been detectable in the experiment. With the SA model there is a conspicuous separation bubble near the trailing edge, as shown in Fig. 13. Since this separation region does not appear in the experiment, it seems to be a consequence of the delayed jet departure on the Coanda surface (separation at approximately $\theta = 124^\circ$).

At the medium C_μ co
sitivity of the results t
with the SST model than
For example, with appro
density in the tangential
nated grid 2, medium
having the same mesh d
foil, we obtained a resul
the jet flow. As seen in

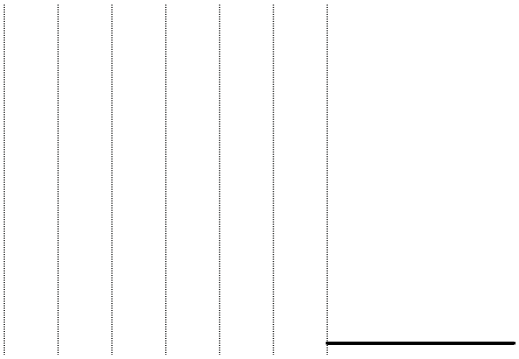

In summary, the μ_t field on grid 2m with the SST model only accounts for a delay in jet separation relative to the other models due to its near-wall behavior. This does not explain why the jet does not separate on the Coanda surface, moving instead onto the lower airfoil surface. For any blowing coefficient C_μ, there apparently is a corresponding jet separation point limit. If the jet flow exceeds that limit, then it moves onto the airfoil lower surface. Of course, once the jet flow gets to the lower surface, the present oncoming flow is not strong enough near the surface to oppose the jet flow. How far the jet moves upstream depends on the C_μ. At the present flow Mach number and with high enough C_μ the jet can actually travel around the airfoil.

In Figs. 17 and 18 velocity profiles upstream of the circular aft section on the upper and lower surfaces computed with the three

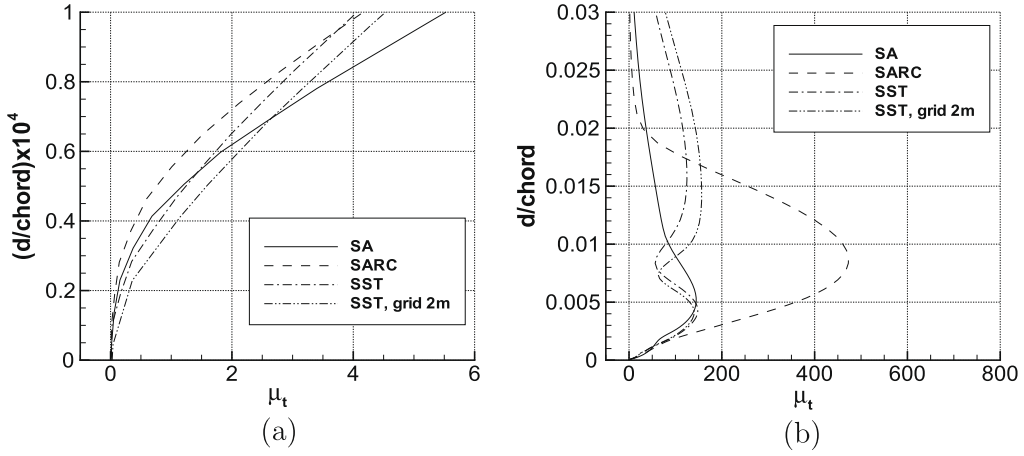

Fig. 16. Turbulent viscosity profiles, $C_\mu = 0.10$, $\theta = 90^\circ$, grid 5m except otherwise indicated: (a) Near surface and (b) Outer region.

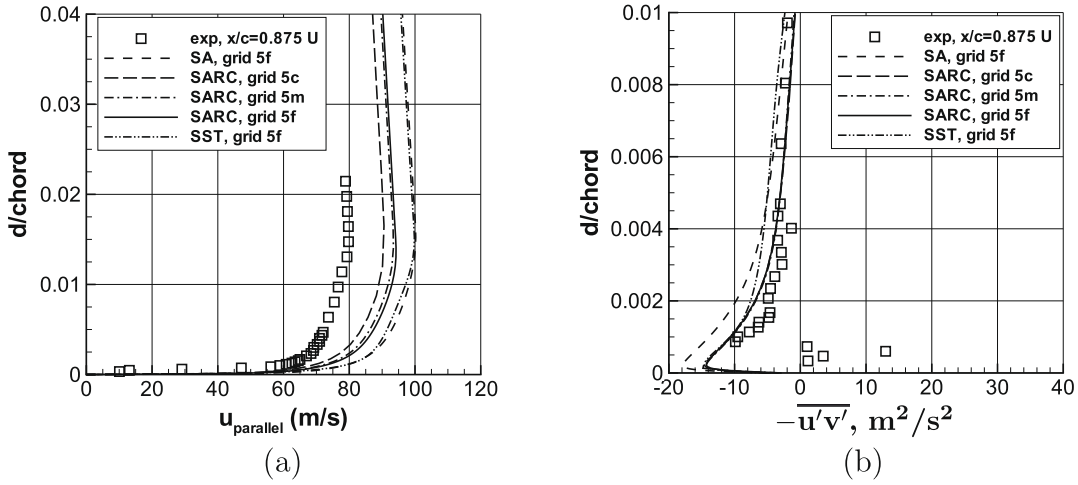

Fig. 17. Velocity and specific Reynolds stress profiles, 3 models, $x/c = 0.875$ on upper surface, $C_\mu = 0.10$, grid 5: (a) Velocity profile, and (b) specific Reynolds stress profile.

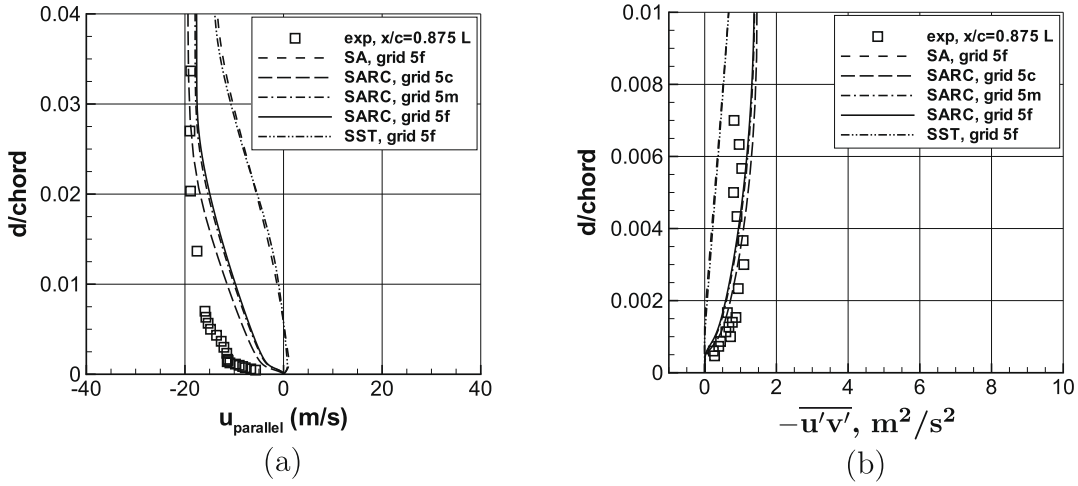

Fig. 18. Velocity and specific Reynolds stress profiles, 3 models, $x/c = 0.875$ on lower surface, $C_\mu = 0.10$, grid 5: (a) Velocity profile and (b) specific Reynolds stress profile (*Note:* Coanda surface coordinate system used).

different turbulence models are compared with the data. Unlike the $C_\mu = 0.03$ case there is a large disagreement with the experimental data at the $x/c = 0.875$ locations on the upper surface of the airfoil. An estimate of the velocity at the edge of the boundary layer based on static and total pressures is not consistent with the measured data. Furthermore, as we will show subsequently, the numerical predictions of the external flow tangential velocity component at the jet exit location are in good agreement with

the measured data. We have also performed a preliminary three-dimensional calculation of the flow over the CC wing in a wind tunnel (see Swanson et al. [5]). The mid-span velocity profile at $x/c = 0.875$ is similar to the profiles of the two-dimensional calculations. Since we have not performed grid resolution studies for this simulation, we can only conclude that the three-dimensional effects do not appear to be strong enough to cause such a significant discrepancy. Based on all these results there is no evident explanation for the difference between the predicted and experimental velocity data on the upper surface at $x/c = 0.875$.

The velocity and shear stress profiles on the Coanda surface computed with the three turbulence models are given in Figs. 19(a–f) and 20(a–f), respectively. Again, the effect of grid density on the profiles determined with the SARC model is also included. The SARC model gives the best agreement with the data, and there are only small differences between the profiles on the

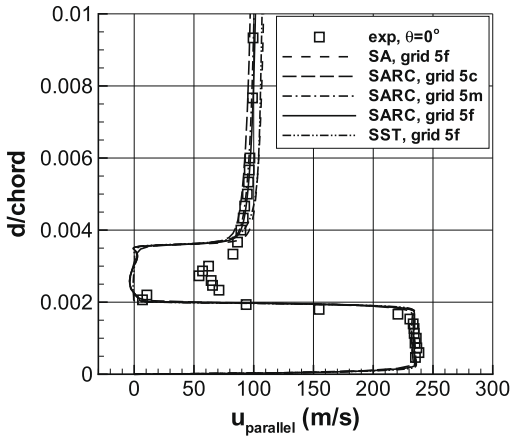

(a) $\theta = 0°$

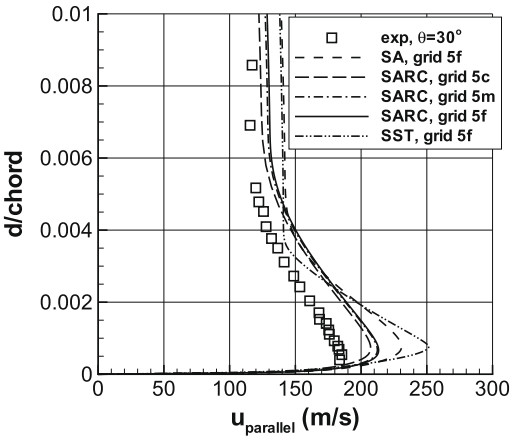

(b) $\theta = 30°$

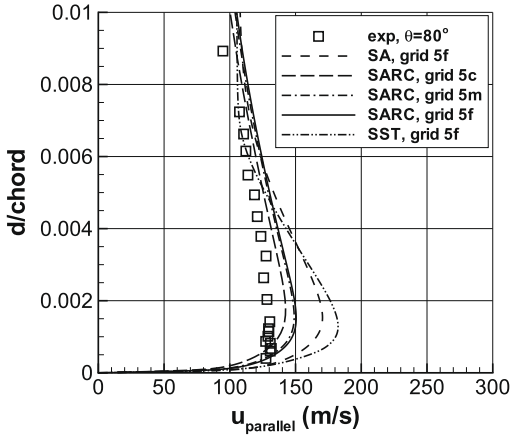

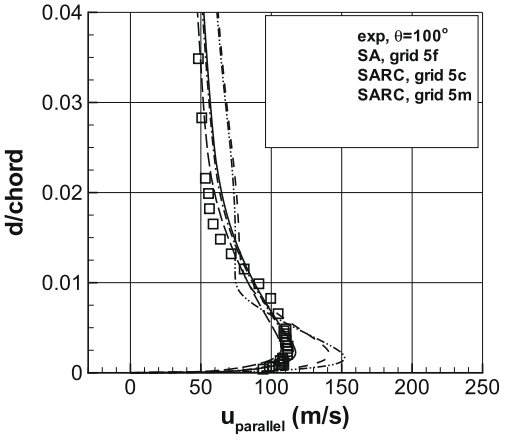

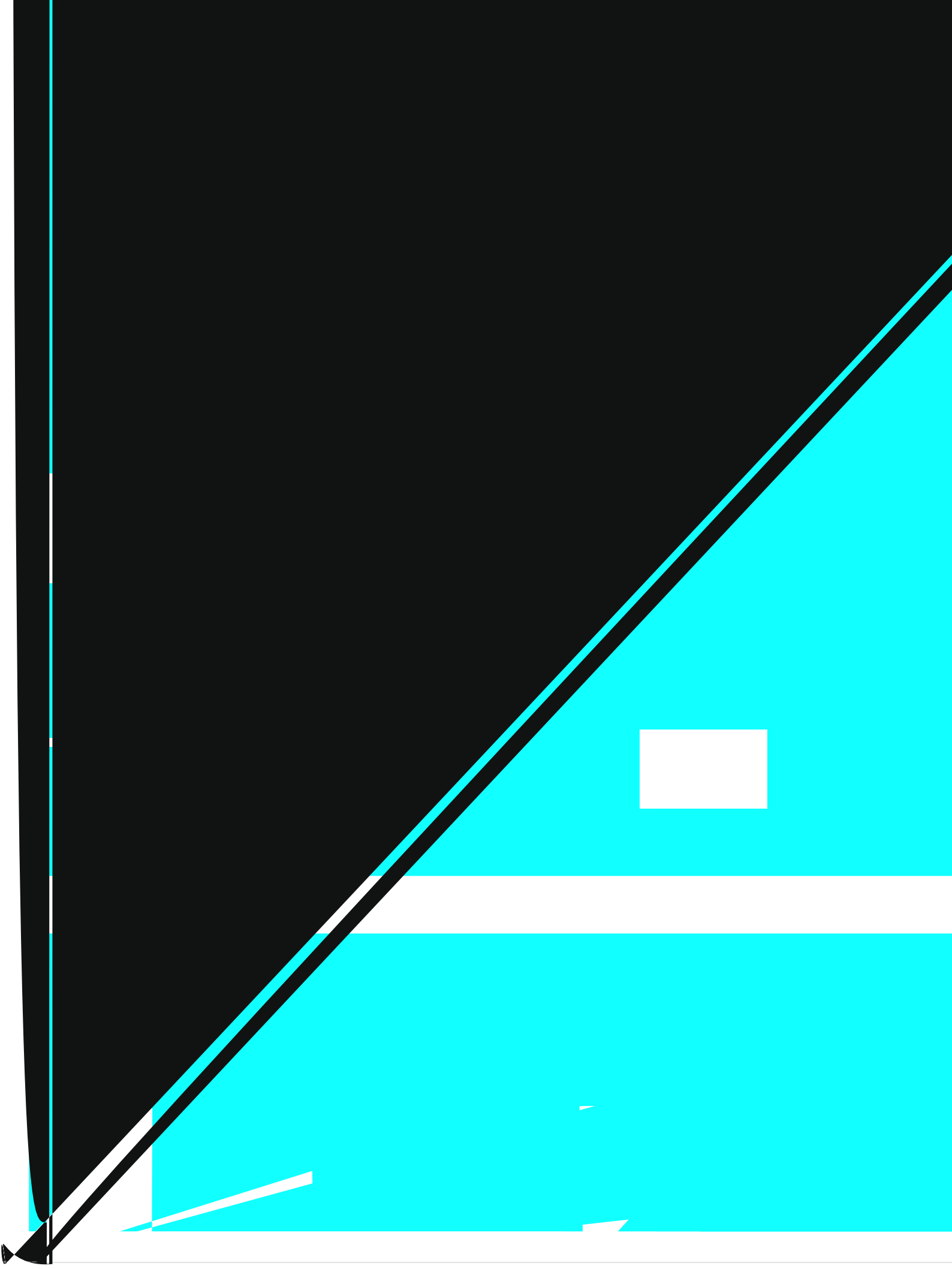

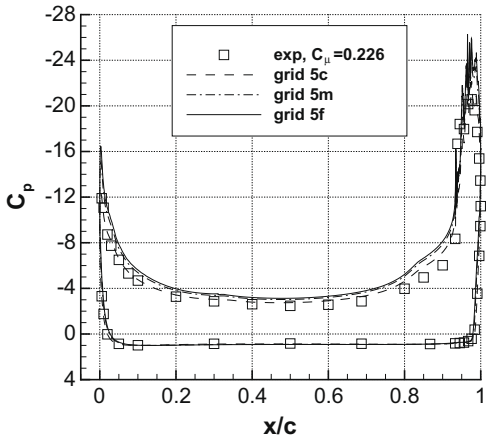

Fig. 21. Comparison of surface pressures computed with SARC model ($M_\infty = 0.12$, $\alpha = -8.94^\circ$, $Re_c = 0.986 \times 10^6$, $C_\mu = 0.226$).

experimental value. This is partly a consequence of the predicted suction peak on the aft end of the airfoil exceeding that of the experiment by about 12%. Unfortunately, for this calculation we have no jet exit velocity to compare against to verify that the actual C_μ of the experiment is being matched. The jet separates at about $\theta = 134^\circ$. Although not shown, the results with both the SA and SST models exhibit nonphysical jet behavior for this case.

7.4. Variation of C_L with C_μ

The variation of the lift coefficient C_L with the jet momentum coefficient C_μ is presented in Fig. 22. Here, we plot only the variation corresponding to the SARC model, since this model is the only one of those considered that did not have a jet wrap-around result for any of the flow conditions. Fig. 22 demonstrates that even though the computed results agree fairly well with the experiment at the lower C_μ, they still significantly overpredict the lift coefficient at higher C_μ. Such a discrepancy in C_L can be caused by delayed separation and/or overprediction of the pressure suction peaks. The lift and drag coefficients for all calculations (and on all grids) having converged solutions are given in Table 2.

8. Concluding remarks

Three low Mach number CC airfoil flows have been computed. With these three cases low, medium, and high values for the jet momentum coefficient have been considered. Three transport-type

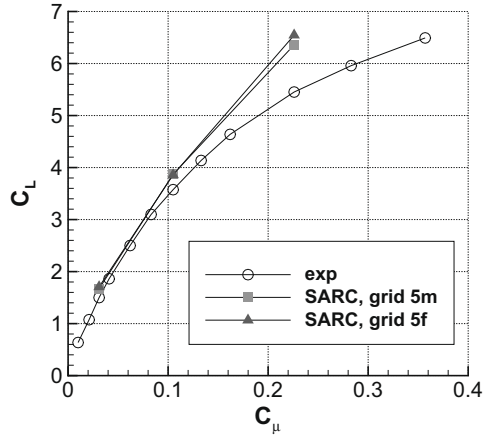

Fig. 22. Variation of lift coefficient with jet momentum coefficient.

Table 2
Comparison of computed and experimental lift coefficients for circulation control airfoil.

Model	C_μ	Grid 5	$(C_L)_{exp}$	C_L	C_D
SA	0.030	Coarse	1.500	1.797	0.02735
	0.030	Medium		1.845	0.02516
	0.030	Fine		1.853	0.02450
SA	0.100	Coarse	3.575	4.109	0.05501
	0.100	Medium		4.421	0.05066
	0.100	Fine		4.480	0.04864
SARC	0.030	Coarse	1.500	1.627	0.02619
	0.030	Medium		1.671	0.02435
	0.030	Fine		1.707	0.02356
SARC	0.100	Coarse	3.575	3.512	0.04921
	0.100	Medium		3.769	0.04583
	0.100	Fine		3.826	0.04449
SARC	0.226	Coarse	5.452	5.833	0.1093
	0.226	Medium		6.359	0.1129
	0.226	Fine		6.546	0.1155
SST	0.030	Coarse	1.500	1.681	0.02572
	0.030	Medium		1.786	0.02458
	0.030	Fine		1.806	0.02469
SST	0.100	Coarse	3.575	4.098	0.05205
	0.100	Medium		4.423	0.05086
	0.100	Fine		4.432	0.05070

equation models for turbulence have been investigated. These models include the one-equation SA model, the SA model with rotation and curvature corrections (SARC), and the SST model of Menter. Comparisons have been made with surface pressures, velocity profiles, specific Reynolds stress profiles, and streamline patterns from the Novak et al. experiment. The effect of mesh density on the solutions has been examined.

The importance of including curvature effects in the turbulence model when computing CC airfoil flows has been demonstrated. For all three CC airfoil flow cases the closest agreement with the experimental surface pressures and streamlines has been obtained with the SARC model. However, at high values of the jet velocity (e.g., $C_\mu = 0.226$), the agreement of the numerical solution with the experimental data deteriorates, reflecting a delayed separation and resulting in a lift coefficient that exceeds the experimental value. There are several possible factors contributing to this deterioration. One is that the jet exit velocity may be too high. Mean velocity measurements are not available for the $C_\mu = 0.226$ case to check this. A second factor is that the α correction does not reduce the effective α enough. Of course, at this higher C_μ, there is the possibility of some significant three-dimensional effects in the experiment due to the tunnel sidewall boundary-layer separation.

For the two jet momentum coefficients $C_\mu = 0.03$ and $C_\mu = 0.10$, the SARC model allows good predictions of the jet departure location on the Coanda surface, but the SA and SST models produce a significant delay in the jet separation relative to that of the experiment. For $C_\mu = 0.226$ the jet computed with the SA and SST models wraps unphysically far around the airfoil. Among the models tested, only the SARC model produces physically realistic solutions at the highest blowing rate.

A number of researchers have encountered non-physical solutions when computing CC airfoil flows with various turbulence models. In these solutions a jet wrap-around occurs, where the jet traverses the entire Coanda surface (circular trailing edge) and at least part of the airfoil lower surface. We have shown that with the SST model insufficient mesh resolution in the tangential direction on the Coanda surface can be at least partially responsible for this solution behavior. However, simple grid refinement does not always cure this problem. We have also examined details of the μ_t when jet wrap-around occurs. Comparing the μ_t values of the three different turbulence models near the wall and upstream of the experimental jet separation location indicates that the

highest values of μ_t occur for the SST model when there is jet wrap-around. There seems to be a jet separation point beyond which the jet flow can travel onto the airfoil lower surface, and then it can readily move upstream if the Mach number of the oncoming flow is low enough.

We have discussed the two primary causes of underprediction of the experimental suction peak on the aft end of a CC airfoil with a circular trailing edge. One cause is setting the momentum flux too low for the inflow boundary condition in the plenum, which results in a too low jet exit velocity (i.e., the computational C_μ condition is too low). The other is performing an incompressible flow simulation when there is a transonic jet flow, which results in a lower acceleration of the jet flow than required. We have demonstrated that using the nominal angle of attack (α) rather than the required effective α can actually compensate for the reduced circulation associated with the underprediction of the suction peak, allowing a good comparison with pressure data over most of the CC airfoil even when solving the "wrong problem".

While the results of this paper are quite encouraging, we should once again emphasize that similar results are not obtained at different flow conditions (e.g., higher values of free-stream Mach number) or with different types of circular trailing edges for CC airfoil flows. This failure to reliably predict these types of flows for a range of conditions is not exclusive to the SARC model. Furthermore, such behavior is not limited to isotropic turbulence models, which use the Boussinesq eddy-viscosity approximation to determine the Reynolds stress tensor. Both the explicit algebraic stress model (EASM) and the full Reynolds stress (FRS) model, which do not invoke the Boussinesq approximation, have also exhibited similar behavior when applied to various CC airfoil flows. Even when physically correct solutions are obtained with a given model, there is usually a significant error in the computed aerodynamic coefficients relative to the experimental data. In addition to the issue of a reliable turbulence model, computational solutions tend to be highly sensitive to numerical parameters and methods of solution. Clearly, the current prediction capability with RANS methods for CC flows over Coanda surfaces is not ready for a general design procedure.

References

[1] Anders SG, Sellers WL, Washburn AE. Active flow control activities at NASA Langley. AIAA Paper 2004–2623;2004.

[2] Jones GS, Englar RJ, Advances in pneumatic-controlled high-lift systems through pulsed blowing. AIAA Paper 2003–3411;2003.

[3] Jones GS, Joslin RD, editors, Proceedings of circulation control workshop. NASA CP 2005–213509, Hampton, Virginia; 2004.

[4] Abramson J. Two-dimensional subsonic wind tunnel evaluation of two related cambered 15-percent circulation control airfoils. DTNSRDC ASED-373;1977.

[5] Swanson RC, Rumsey CL, Anders SG. Aspects of numerical simulation of circulation control airfoils. Applications of Circulation Control Technologies. In: Joslin RD, Jones GS, editors. Progress in astronautics and aeronautics, vol. 214. AIAA; 2006. p. 469–98.

[6] Krist SL, Biedron RT, Rumsey CL. CFL3D user's manual. NASA TM-1998–208444;1998.

[7] Abramson J, Rogers E. High-speed characteristics of circulation control airfoils. AIAA Paper 83–0265;1983.

[8] Spalart PR, Allmaras SR. A one-equation turbulence model for aerodynamic flows. La Recherche Aerospatiale 1994;1:5–21.

[9] Spalart PR, Shur M. On the sensitization of turbulence models to rotation and curvature. Aerospace Sci Technol 1997;5:297–302.

[10] Menter FR. Two-equation eddy-viscosity turbulence models for engineering applications. AIAA J 1994;32(8):1598–605.

[11] Rumsey CL, Gatski TB, Morrison JH. Turbulence model predictions of strongly curved flow in a U-duct". AIAA J 2000;38(8):1394–402.

[12] Fasel HF, Gross A, Wernz S. Investigation of turbulent Coanda wall jets using DNS and RANS. Applications of Circulation Control Technologies. In: Joslin RD, Jones GS, editors. Progress in astronautics and aeronautics, vol. 214. AIAA; 2006. p. 401–20.

[13] Wilcox DC. Reassessment of the scale-determining equation for advanced turbulence models. AIAA J 1988;26:1299–310.

[14] Wilcox DC. Turbulence modeling for CFD. 2nd ed. DCW Industries, Inc.; 1998.

[15] Chang III PA, Slomski J, Marino T, Ebert MP. Full Reynolds stress modeling of circulation control airfoils. Applications of Circulation Control Technologies, In: Joslin RD, Jones GS, editors. Progress in astronautics and aeronautics, vol. 214; AIAA; 2006. p. 445–66.

[16] Launder B, Reece G, Rodi W. Progress in the development of a Reynolds stress model. J Fluid Mech 1975;68(3):537–66.

[17] Novak CJ, Cornelius KC, Roads RK. Experimental investigations of the circular wall jet on a circulation control airfoil. AIAA Paper 87–0155;1987.

[18] Shrewsbury GD. Numerical evaluation of circulation control airfoil performance using Navier–Stokes methods. AIAA Paper 86–0286;1986.

[19] Shrewsbury GD. Numerical study of a research circulation control airfoil using Navier–Stokes methods. J Aircraft 1989;26(1):29–34.

[20] Viegas JR, Rubesin MW, MacCormack RW. On the validation of a code and a turbulence model appropriate for circulation control airfoils, AGARD, validation of computational fluid dynamics, vol. 1. Symposium Papers and Round Table Discussion; 1988.

[21] Baldwin BS, Lomax H. Thin layer approximation and algebraic model for separated flows. AIAA Paper 78–257;1978.

[22] Swanson RC, Rumsey CL, Anders SG. Progress towards computational method for circulation control airfoils. AIAA Paper 2005–0089;2005.

[23] Robinson DF, Hassan HA. Further development of the $k-\zeta$ (enstrophy) turbulence closure model. AIAA J 1998;36(10):1825–33.

[24] Baker WJ, Paterson EG. RANS CFD simulation of a circulation-control foil: validation of performance, flow field, and wall jet. AIAA Paper 2006–3010;2006.

[25] Paterson E, Wilson R, Stern F. General-purpose parallel unsteady RANS ship hydrodynamics code, Tech. Report 432, IIHR Hydroscience and Engineering, The University of Iowa, Iowa City, Iowa; 2003.

[26] AcuSolve Commands Reference Manual v1.7 [computer program], ACUISM Software Inc. (http://www.acusim.com), Mountain View, California, 2005.

[27] Shakib F. Finite element analysis of the compressible Euler and Navier–Stokes equations, Ph.D. Thesis, Stanford University, Palo Alto, California; 1989.

[28] Pfingsten K-C, Jensch C, Korber W, Radespiel R. Numerical simulation of the flow around circulation control airfoils, First CEAS European Air and Space Conference, Berlin, Germany; 2007.

[29] Gerhold T. Overview of the hybrid RANS code TAU, MEGAFLOW – Numerical Flow Simulation for Aircraft Design, vol. 89. Springer-Verlag, 2005 (Notes on Numerical Fluid Mechanics and Multidisciplinary Design) 81–92.

[30] Novak CJ, Cornelius KC. Advanced airfoil performance and analysis, vol. II: experimental program summary, Lockheed Report L87R0618; 1987.

[31] Wood NJ, Rogers EO. An estimation of the wall interference on a two-dimensional circulation control airfoil, AIAA Paper 86–0738;1986.

[32] Roe P. Approximate Riemann solvers, parameter vectors, and difference schemes. J Comp Phys 1981;43:357–72.

[33] Rumsey CL, Gatski TB, Anderson WK, Nielsen EJ. Isolating curvature effects in computing wall-bounded turbulent flows. Int J Heat Fluid Flow 2001;22:573–82.

[34] Menter FR. Improved two-equation $k-\omega$ turbulence model for aerodynamic flows. NASA TM 103975;1992.

[35] Menter FR. Zonal two equation $k-\omega$ turbulence model for aerodynamic flows. AIAA Paper 93–2906;1993.

[36] Swanson RC, Rumsey CL. Numerical issues for circulation control calculations. AIAA Paper 2006–3008;2006.

[37] Mani M, Ladd JA, Bower WW. Rotation and curvature assessment for one- and two-equation turbulence models. J Aircraft 2004;41(2):268–73.